



Conservation and Rewiring of Functional Modules Revealed by an Epistasis Map in Fission Yeast

Assen Roguev, *et al.*
Science **322**, 405 (2008);
DOI: 10.1126/science.1162609

The following resources related to this article are available online at www.sciencemag.org (this information is current as of October 27, 2008):

Updated information and services, including high-resolution figures, can be found in the online version of this article at:

<http://www.sciencemag.org/cgi/content/full/322/5900/405>

Supporting Online Material can be found at:

<http://www.sciencemag.org/cgi/content/full/1162609/DC1>

This article **cites 40 articles**, 16 of which can be accessed for free:

<http://www.sciencemag.org/cgi/content/full/322/5900/405#otherarticles>

This article appears in the following **subject collections**:

Genetics

<http://www.sciencemag.org/cgi/collection/genetics>

Information about obtaining **reprints** of this article or about obtaining **permission to reproduce this article** in whole or in part can be found at:

<http://www.sciencemag.org/about/permissions.dtl>

Conservation and Rewiring of Functional Modules Revealed by an Epistasis Map in Fission Yeast

Assen Roguev,^{1,2} Sourav Bandyopadhyay,³ Martin Zofall,⁴ Ke Zhang,⁴ Tamas Fischer,⁴ Sean R. Collins,^{1,2,5} Hongjing Qu,^{1,2} Michael Shales,^{1,2} Han-Oh Park,⁶ Jacqueline Hayles,⁷ Kwang-Lae Hoe,⁸ Dong-Uk Kim,⁸ Trey Ideker,^{3*} Shiv I. Grewal,^{4*} Jonathan S. Weissman,^{1,2,5*} Nevan J. Krogan^{1,2*}

An epistasis map (E-MAP) was constructed in the fission yeast, *Schizosaccharomyces pombe*, by systematically measuring the phenotypes associated with pairs of mutations. This high-density, quantitative genetic interaction map focused on various aspects of chromosome function, including transcription regulation and DNA repair/replication. The E-MAP uncovered a previously unidentified component of the RNA interference (RNAi) machinery (*rsh1*) and linked the RNAi pathway to several other biological processes. Comparison of the *S. pombe* E-MAP to an analogous genetic map from the budding yeast revealed that, whereas negative interactions were conserved between genes involved in similar biological processes, positive interactions and overall genetic profiles between pairs of genes coding for physically associated proteins were even more conserved. Hence, conservation occurs at the level of the functional module (protein complex), but the genetic cross talk between modules can differ substantially.

Genetic interactions report on the extent to which the function of one gene depends on the presence of a second. This phenomenon, known as epistasis, can be used for defining functional relationships between genes and the pathways in which the corresponding proteins function. Two main categories of genetic interactions exist: (i) negative (e.g., synthetic sickness/lethality) and (ii) positive (e.g., suppression). We have developed a quantitative approach, termed epistasis map (E-MAP), allowing us to measure the whole spectrum of genetic interactions, both positive and negative (1, 2). In budding yeast, *Saccharomyces cerevisiae*, it has been demonstrated that positive genetic interactions can identify pairs of genes whose products are physically associated and/or function in the same pathway (1, 2), whereas negative interactions exist between genes acting on parallel pathways (3, 4).

We developed the Pombe Epistasis Mapper (PEM) approach (5) that allows high-throughput

generation of double mutants in the fission yeast, *Schizosaccharomyces pombe*. Fission yeast is more similar to metazoans than is *S. cerevisiae*, owing to its large complex centromere structure, the restriction of spindle construction to mitotic entry, gene regulation by histone methylation and chromodomain heterochromatin proteins, gene and transposon regulation by the RNA interference (RNAi) pathway, and the widespread presence of introns in genes. To further study these processes and to try to understand how genetic interaction networks have evolved (6), we generated an E-MAP in *S. pombe* that focuses on nuclear function, designed to be analogous to one we created in budding yeast (2).

An E-MAP in *S. pombe*. Using our PEM system (5), we generated a quantitative genetic interaction map in *S. pombe*, comprising ~118,000 distinct double mutant combinations among 550 genes involved in various aspects of chromosome function (Fig. 1A and tables S1 and S4) (7). The genes on the map were chosen on the basis of a previous budding yeast E-MAP (1, 2) and also included factors present in human (but not in *S. cerevisiae*), including the RNAi machinery. We used colony size (measured from high-density arrays) as a quantitative phenotypic read-out to compute a genetic interaction score (S score) and previously described quality control measures to ensure a high-quality data set (7, 8) (fig. S1A).

We have previously observed two prominent general trends between genetic interactions and protein-protein interactions (PPIs): (i) a propensity for positive genetic interactions and (ii) strong correlations of genetic interaction profiles between genes coding for proteins participating

in PPIs (2). Using a high-confidence set of 151 PPI pairs from *S. pombe* (9) (table S2), we observed the same trends in this organism (Fig. 1, B and C). Thus, it appears these relationships are evolutionarily conserved and may represent a general feature of biological networks.

Exploring nuclear function in fission yeast.

We generated a highly structured representation of the genetic map by subjecting the data to hierarchical clustering (Fig. 2). By scrutinizing several interaction-rich regions, we were able to recapitulate known, and identify previously unknown, functional relationships.

Genes required for DNA repair/recombination and various checkpoint functions form clusters enriched in negative interactions (Fig. 2, region 1). The *rad9-hus1-rad1* (9-1-1) checkpoint complex (10) clusters together with *rad17* (the homolog of budding yeast *RAD24*), which loads it onto DNA (11). We found two genes linked to tRNA biogenesis, *sen1* and *trm10*, within the DNA repair cluster. tRNA regulation has been linked to the DNA damage response pathway in *S. cerevisiae* (12), and these genetic patterns suggest that a similar mechanism may exist in fission yeast. To genetically interrogate the function of essential genes, we used the decreased abundance by mRNA perturbation (DAmP) strategy for generating hypomorphic alleles (1) (table S1) and found that the DAmP allele of *mcl1*, involved in DNA replication control and repair, is highly correlated with components of the replication checkpoint (*mrc1* and *csn3*).

The fission yeast homologs of the components of the SWR complex (SWR-C)—which, in budding yeast, incorporates the histone H2A variant Htz1 (Pht1 in fission yeast) into chromatin (13–15)—form a highly correlated group (Fig. 2, region 2). A jumonji domain-containing protein, *Msc1*, whose *S. cerevisiae* ortholog *ECM5* is not part of the budding yeast's SWR-C, is found within the fission yeast SWR-C cluster, consistent with the demonstration that *Msc1* acts through Pht1 to promote chromosome stability (16).

The E-MAP reveals functional specialization of the fission yeast Set1 histone H3 lysine 4 methyltransferase complex (SET1-C, COMPASS) (17–20). In *S. pombe*, five of its subunits (core SET1-C: *set1*, *spp1*, *swd1*, *swd21*, and *swd3*) are indispensable for H3-K4 methylation (19) and form a highly correlated cluster on the E-MAP (Fig. 2, region 3). In budding yeast, another component of COMPASS, *Swd2*, is essential and is part of two distinct complexes: (i) SET1-C and the (ii) Cleavage and Polyadenylation Factor (CPF) (17, 21). *S. pombe* contains two nonessential paralogs of *SWD2* (*swd21* and *swd22*), which have previously been shown to act independently in the *S. pombe* SET1-C and CPF, respectively (22). Consistent with this observation, on our map, *swd21* is part of the core SET1-C, whereas *swd22* is strongly correlated with the *SSU72* ortholog, a part of CPF (21, 23) (Fig. 2, region 3).

¹Department of Cellular and Molecular Pharmacology, University of California, San Francisco, CA 94158, USA. ²California Institute for Quantitative Biosciences, University of California, San Francisco, CA 94158, USA. ³Department of Bioengineering and Program in Bioinformatics, University of California–San Diego, La Jolla, CA 92093, USA. ⁴Laboratory of Biochemistry and Molecular Biology, Center for Cancer Research, National Cancer Institute, NIH, Bethesda, MD 20892, USA. ⁵Howard Hughes Medical Institute, San Francisco, CA 94158, USA. ⁶Bioneer Corporation, Daejeon, Korea. ⁷Cell Cycle Laboratory, Cancer Research UK, London Research Institute, 44 Lincoln's Inn Fields, London WC2A 3PX, UK. ⁸Genomic Research Center, Korea Research Institute of Bioscience and Biotechnology, Daejeon, Korea.

*To whom correspondence should be addressed. E-mail: trey@bioeng.ucsf.edu (T.I.); grewals@mail.nih.gov (S.I.G.); weissman@cmp.ucsf.edu (J.S.W.); krogan@cmpmail.ucsf.edu (N.J.K.)

The Ash2-Sdc1 heterodimer within the SET1-C also behaves differently. In *S. cerevisiae*, its orthologous pair (Bre2p-Sdc1p) is exclusively found in the SET1-C (17), whereas in fission yeast it is shared between the SET1-C and LID2-C (19). Consistent with this result, the dimer does not cluster next to core Set1-C [as is observed in budding yeast (2)] but is more similar to *snt2*, a member of LID2-C (Fig. 2, region 3).

Genetic dissection of the RNAi pathway.

The RNAi pathway in *S. pombe* is composed of several components, including CLR4-C, RDR-C, RITS, dicer (Dcr1), and the HP1 homolog Swi6 (24). All known components of the RNAi machinery that were analyzed cluster next to each other and primarily display positive genetic interaction with one another (Fig. 3A). Within this cluster are subclusters corresponding to the different protein complexes. Consistent with previous reports, we found positive genetic interactions between the RNAi machinery and *epe1*, an anti-silencing factor involved in the transcription of heterochromatic regions by RNA polymerase II (RNAPII) (25) and required for RNAi-mediated heterochromatin assembly (24). Conversely, we found negative interactions between RNAi components involved in posttranscriptional gene silencing and factors implicated in transcriptional gene silencing (TGS) of repeat sequences and other loci. In particular, *clr3*, a histone deacetylase and catalytic subunit of the Snf2/Hdac-containing repressor complex (26) that is involved in TGS at centromeric repeats (24) and Tf2 retrotransposons (27, 28), shows negative interactions with RNAi components (Fig. 3A).

Within the RNAi cluster, we also found a previously unknown component of the RNAi pathway, SPCC1393.05, which we named *rsh1* (involved in RNAi silencing and heterochromatin formation) (Fig. 3A). The gene encodes a 110-kD protein with no obvious homologs or

apparent sequence motifs. We used chromatin immunoprecipitation to determine that Rsh1 is localized to heterochromatic centromeric regions. Its absence causes a substantial reduction of silencing at these loci and a loss of small interfering RNAs (siRNAs) expressed from the centromeric dg/dh repeats (Fig. 3, B to F). Additionally, *rsh1Δ* leads to a marked reduction of H3-K9 dimethylation and Swi6/HP1 binding that correlates with lowered levels (more than sixfold decrease) of Ago1 (a component of RITS) recruitment to the outer (*otr*) centromeric repeat region (Fig. 3, G and H).

We also observed positive interactions between the RNAi machinery and homologs of factors involved in the transition between transcriptional initiation and elongation, including *rpb9* and *iwr1*, components of RNAPII (21, 29), and the Mediator complex (*pmc2*, *rox3*, *pmc5*, and *med2*) (30, 31). Deletions of *rpb9*, *rox3*, *pmc5*, or *pmc2* lead to moderate loss of silencing at the centromere (Fig. 3, I and J).

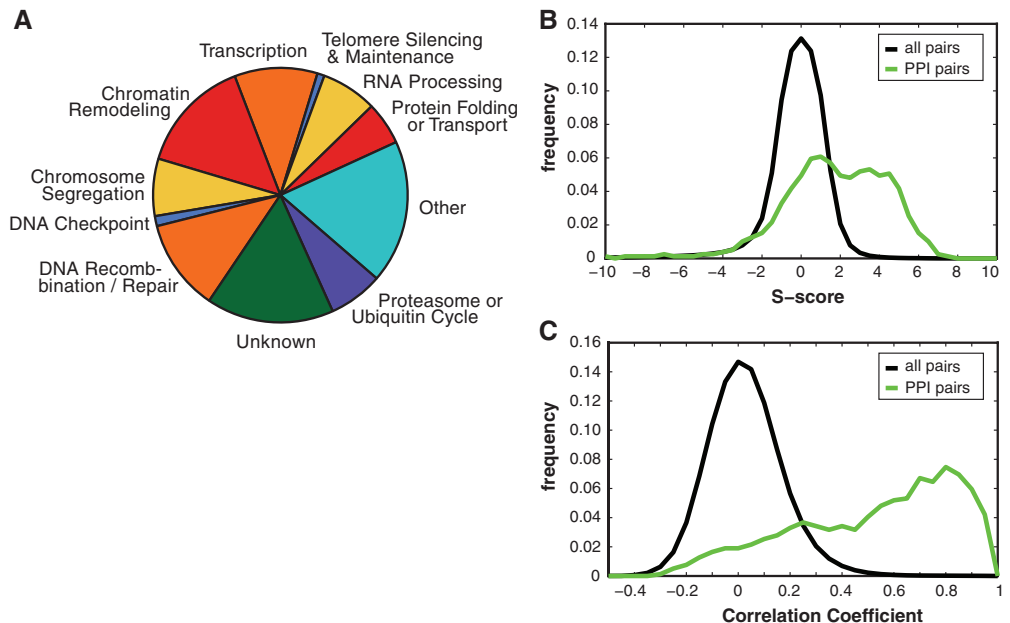
We observed numerous negative genetic interactions between the RNAi machinery and other cellular complexes and processes (Fig. 3A), including the spindle-checkpoint pathway (*mad1*, *mad2*, *bub3*, and *alp14*) (32); components of the DASH complex (33) (*dad1*, *dad2*, *ask1*, and *spc34*); and *mal3*, *tub1*, and *alp31* involved in microtubule stability (34), consistent with the involvement of RNAi/heterochromatin apparatus in proper chromosome segregation (35). The acetyltransferase complex Elongator (36) interacts negatively with the RNAi machinery and clusters next to factors regulating spindle function, consistent with the observation that Elongator may be responsible for tubulin acetylation, required for microtubule-based protein trafficking (37). Finally, components of the DNA repair, checkpoint, and recombination apparatus display negative genetic interactions with the RNAi machinery, suggesting

that the RNAi pathway is also involved in maintaining genomic stability.

Conservation of modular organization of genetic interaction networks. The large evolutionary distance between *S. cerevisiae* and *S. pombe* [~400 million years (38)] allowed us to study the evolution of genetic interactomes. We directly compared the data from this *S. pombe* E-MAP to an analogous database from *S. cerevisiae* (database S4) (2). The overlap of one-to-one annotated orthologs (39) between the two E-MAPs encompasses 239 genes (table S3). First, we analyzed individual negative pairwise interactions in the two organisms. Recently, it has been suggested (6) that negative interactions between yeast and *Caenorhabditis elegans* were not conserved. Although not strong, we did find a conservation of negative interactions (17.3% for S score ≤ -2.5), which became more pronounced (33%) when the analysis was restricted to genes that shared the same functional annotations (Fig. 4A and fig. S2B). To confirm this observation, we used an independent data set from BioGRID (9) and observed similar conservation rates [18% for all and 31% among functionally related genes (7)]. Part of the discrepancy seen in *C. elegans* could be due to functional redundancy, multicellularity, or incomplete knockdowns by RNAi. Furthermore, this comparison was not restricted to functionally related genes (6). In our analysis, we also found a very strong conservation (>50%) of positive interactions (S score ≥ 2.0) [that were not considered by (6)] between pairs of genes whose corresponding proteins are physically associated (Fig. 4A and fig. S2, A to D) (7).

The set of genetic interactions for a given gene provides a sensitive phenotypic signature or profile. Although a global comparison of all correlations of genetic profiles between orthologous pairs in each species (table S3)

Fig. 1. Data set overview. (A) Functional classification of the genes contained within the *S. pombe* E-MAP. The map contains 550 genes that were classified into 11 functional categories (table S4). **(B)** Distribution of interaction scores for pairs of genes corresponding to physically interacting proteins (green) and noninteracting proteins (black). **(C)** Distribution of Pearson correlation coefficients of the genetic interaction profiles for the same set of genes used in (B). For a complete list of PPIs used in this analysis, see table S2.



revealed a weak overall conservation (correlation coefficient $r = 0.14$) (Fig. 4B), pairs corresponding to PPIs were much more highly correlated ($r = 0.60$) (Fig. 4B). An aggregate measure for the likelihood of two proteins to carry out a common function, many of which correspond to PPI pairs, is the complex or linear pathway (COP) score (δ), which integrates the individual genetic interaction score and correlation coefficient of genetic interaction profiles. Pairs of genes displaying high COP scores in both organisms almost exclusively correspond to PPIs (fig. S2E).

To further explore the extent of conservation of genetic networks, the profiles of each of the 239 orthologs in both species were compared to all profiles from the other organism (Fig. 4C). We found some conservation between direct orthologs ($P = 8 \times 10^{-20}$), suggesting that genetic interaction profiles of orthologs across species tend to be similar (fig. S2F). There is,

however, a stronger conservation of genetic profiles between a gene and the ortholog of its interacting partner when only co-complex members were considered (Fig. 4C) ($P = 9 \times 10^{-51}$). Thus, genetic profiles of members of PPI pairs tend to correlate better, not only to their interaction partners within the same species, but also to the orthologs of their interaction partner in an evolutionarily distant organism.

Collectively, these data demonstrate that genetic interactions between particular subsets of genes are conserved between *S. cerevisiae* and *S. pombe*. Specifically, we find conservation of negative interactions when genes involved in the same cellular process are considered. Better conserved are positive interactions and genetic profiles of genes whose products are physically associated. Therefore, we argue that conservation primarily exists at the level of the functional module (protein complex), and perhaps PPIs pose a constraint on functional divergence in evolution.

Rewiring of conserved functional modules.

Biological modules can be defined as highly interconnected groups of physically or functionally associated factors, and they often correspond to protein complexes. In addition to identifying functional modules, high-density genetic interaction data reports on the functional relationships between modules (i.e., the wiring of the network).

To compare the genetic cross talk between modules in the two organisms, we merged and clustered the genetic interaction matrix of *S. pombe* with that of *S. cerevisiae* for the 239 1:1 orthologs (database S2). Inspection of this database revealed a partial overlap of negative interactions between protein complexes (Fig. 5A). For example, in both organisms, SWR-C display negative genetic interactions with the SET1-C and the histone deacetylase (HDAC) complex, SET3-C. However, substantial differences were found as well. For instance, only in budding yeast are there

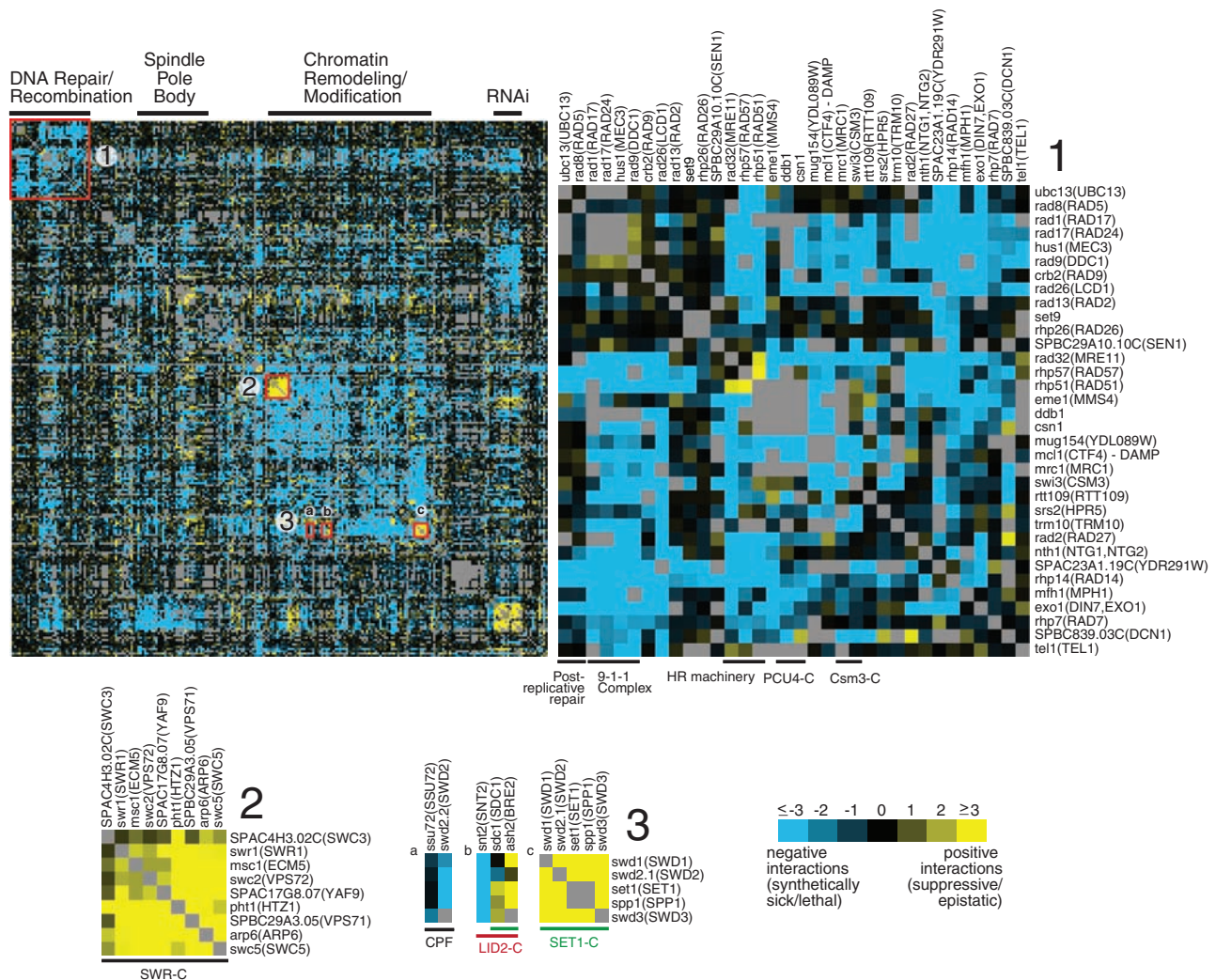


Fig. 2. The *S. pombe* chromosome function E-MAP. A section of the E-MAP with specific regions of interest annotated. Further highlighted are the factors involved in DNA repair/recombination (1), as well as two complexes contained within the chromatin remodeling/modification region: the SWR-C chromatin

remodeling complex (2) and the Set1, Lid2, and CPF complexes (3). The names of the budding yeast orthologs are shown in parentheses (table S3). The final data set consists of 118,575 measurements and contains 5772 negative (S score ≤ -2.5) and 1812 positive (S score ≥ 2) interactions.

negative interactions between SWR-C and components of the spindle checkpoint, the chaperone complex Prefoldin, the HDAC complex, Rpd3C(L), and Mediator (Fig. 5A).

Several possible explanations can be offered. First, the additional subunit unique to the fission yeast SWR-C, Msc1, may alter the function of the complex. Also, species-specific posttranslational modifications may result in different genetic behavior. Msc1 has been shown to harbor ubiquitin ligase activity (40) and may

be involved in ubiquitinating proteins related to the function of SWR-C. Another reason could be the presence or absence of particular cellular machinery. For example, the rewiring of the genetic space surrounding the SWR-C in *S. pombe* may be due to the presence of the RNAi machinery, which shows negative interactions with the complex (Fig. 5B). Consequently, dramatic alterations in the network topology of budding yeast may have been necessary to compensate for the absence of the RNAi path-

way. We cannot rule out the possibility that many of the interactions do exist under different environmental conditions. Nonetheless, a major rewiring of other complexes [e.g., the histone regulatory (HIR) chromatin assembly complex and Prefoldin] (fig. S3) was also observed under the conditions used.

The modularity of biological networks is believed to be one of the main contributors to their robustness, as it implies enhanced functional flexibility. Much like an electronic cir-

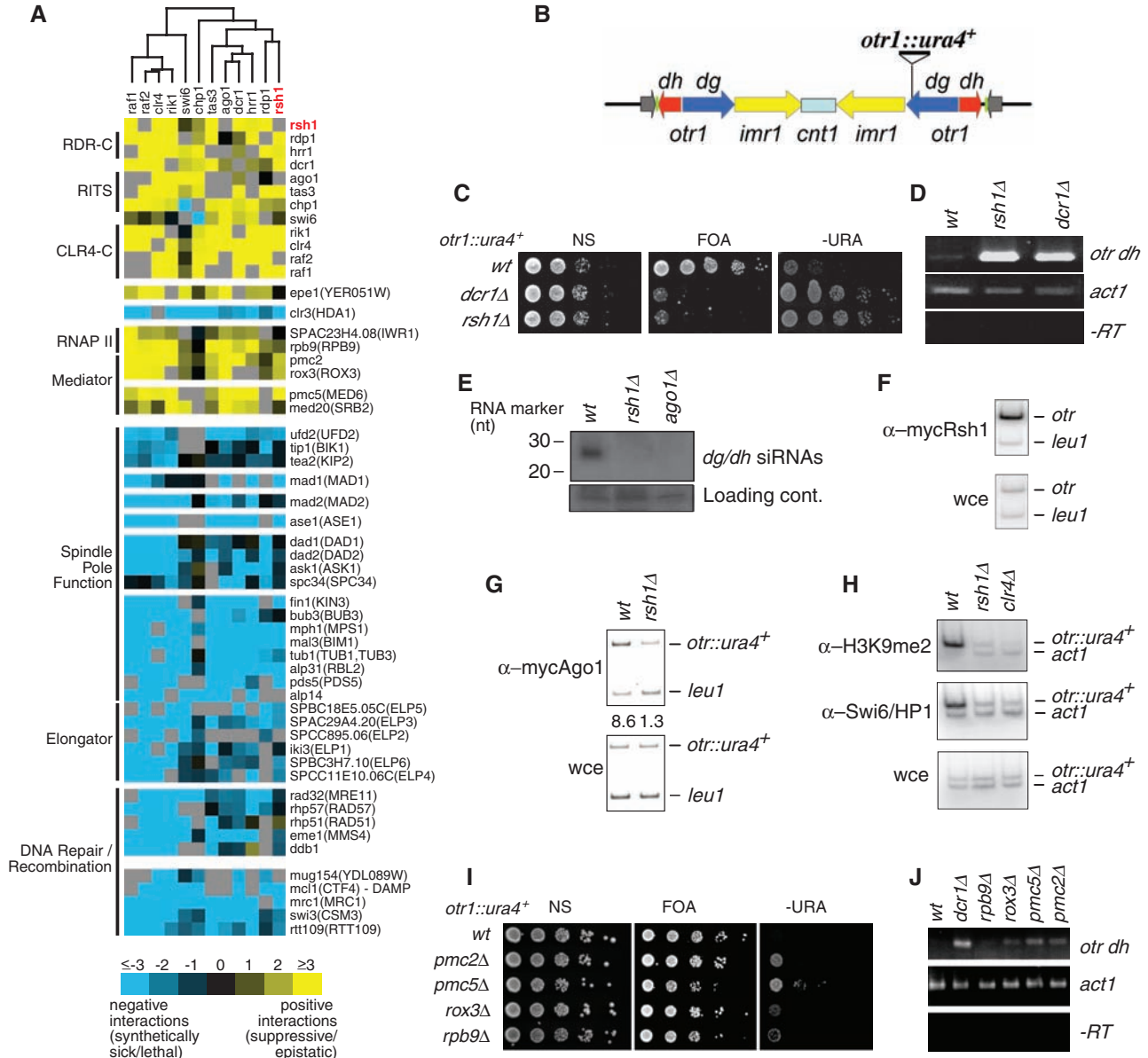


Fig. 3. Characterization of genes involved in the RNAi pathway. **(A)** Genetic profiles for genes involved in RNAi with individual protein complexes or processes annotated. **(B)** Schematic of the centromeric region of chromosome 1 with the position of the *ura4⁺* reporter gene within the *otr1* region. **(C)** Loss of Rsh1p abolishes heterochromatic silencing of the *ura4⁺* reporter gene inserted at the outer repeat region of centromere 1 (*otr1::ura4⁺*). NS, nonselective; FOA, counterselective; -URA, uracil-deficient media. **(D)** Levels of *dh* transcripts analyzed by reverse transcription polymerase chain reaction (RT-PCR) using RNA prepared from indicated strains. **(E)** Loss of siRNAs derived from *dg/dh* repeats in *rsh1*Δ detected by Northern blotting. nt, nucleotides. **(F)** Rsh1 localizes to

outer (*otr*) centromeric repeats. An epitope-tagged version of Rsh1 (mycRsh1) was used to perform chromatin immunoprecipitation (ChIP). wce, whole-cell extract. **(G)** Rsh1 is required for localization of Ago1. Localization of mycAgo1 at *otr1::ura4⁺* in wild-type and *rsh1*Δ cells was assayed using ChIP. *leu1* is an internal loading control for ChIP experiments. **(H)** Effect of *rsh1*Δ on heterochromatin assembly at centromeric repeats. Levels of histone H3 lysine 9 dimethylation (H3K9me2) and Swi6/HP1 at *otr1::ura4⁺* were assayed using ChIPs. **(I and J)** Loss of Mediator and RNAPII subunits affects centromeric silencing. The levels of transcripts corresponding to *dh* centromeric repeats were analyzed by RT-PCR. *leu1* and *act1* are used as internal loading controls.

cuit, such modular architecture allows different tasks to be accomplished with the same minimal set of components by changing the wiring (or

flow of information) between them. Rewiring because of addition or removal of modules allows for economical design of sophisticated networks

that are able to adapt to different conditions and environmental niches at a low cost. We observe this behavior derived from high-density genetic-

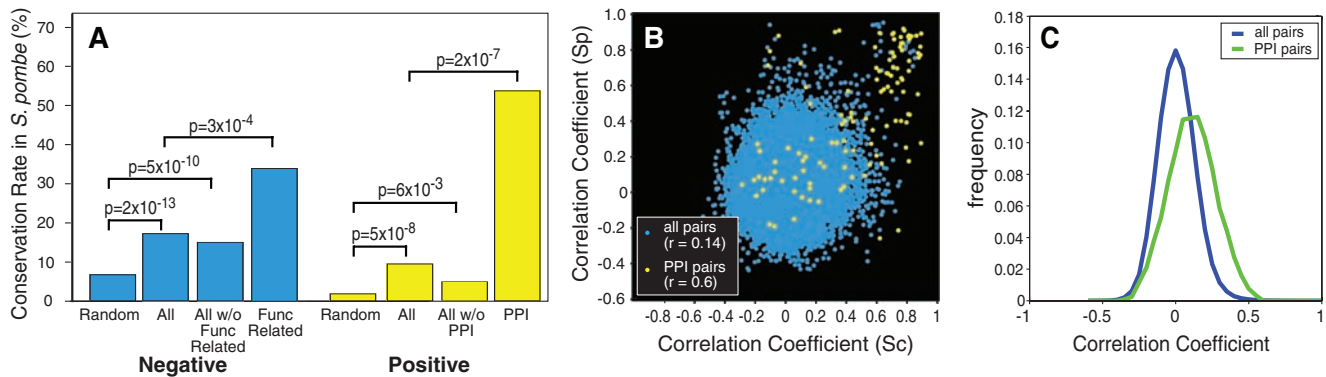


Fig. 4. Modular conservation of genetic interaction patterns. A set of 239 one-to-one orthologs (table S3) was used for the analysis. **(A)** Conservation of positive and negative genetic interactions based on comparison with *S. cerevisiae*. Conservation rates are higher for the subset of negative interactions between genes with the same functional annotation and the subset of positive interactions corresponding to known PPIs in *S. cerevisiae*. Pairs of genes whose

proteins are physically associated or functionally related did not contribute significantly to the general trends (second bar), because removal of these pairs (third bar) resulted in similar conservation rates. *P* values were determined using a two-sided Student's *t* test (7). **(B)** Scatter plot of Pearson correlation coefficients of genetic interaction profiles. Sc, *S. cerevisiae*; Sp, *S. pombe*. **(C)** Distribution of the cross-species Pearson correlation coefficient of genetic profiles.

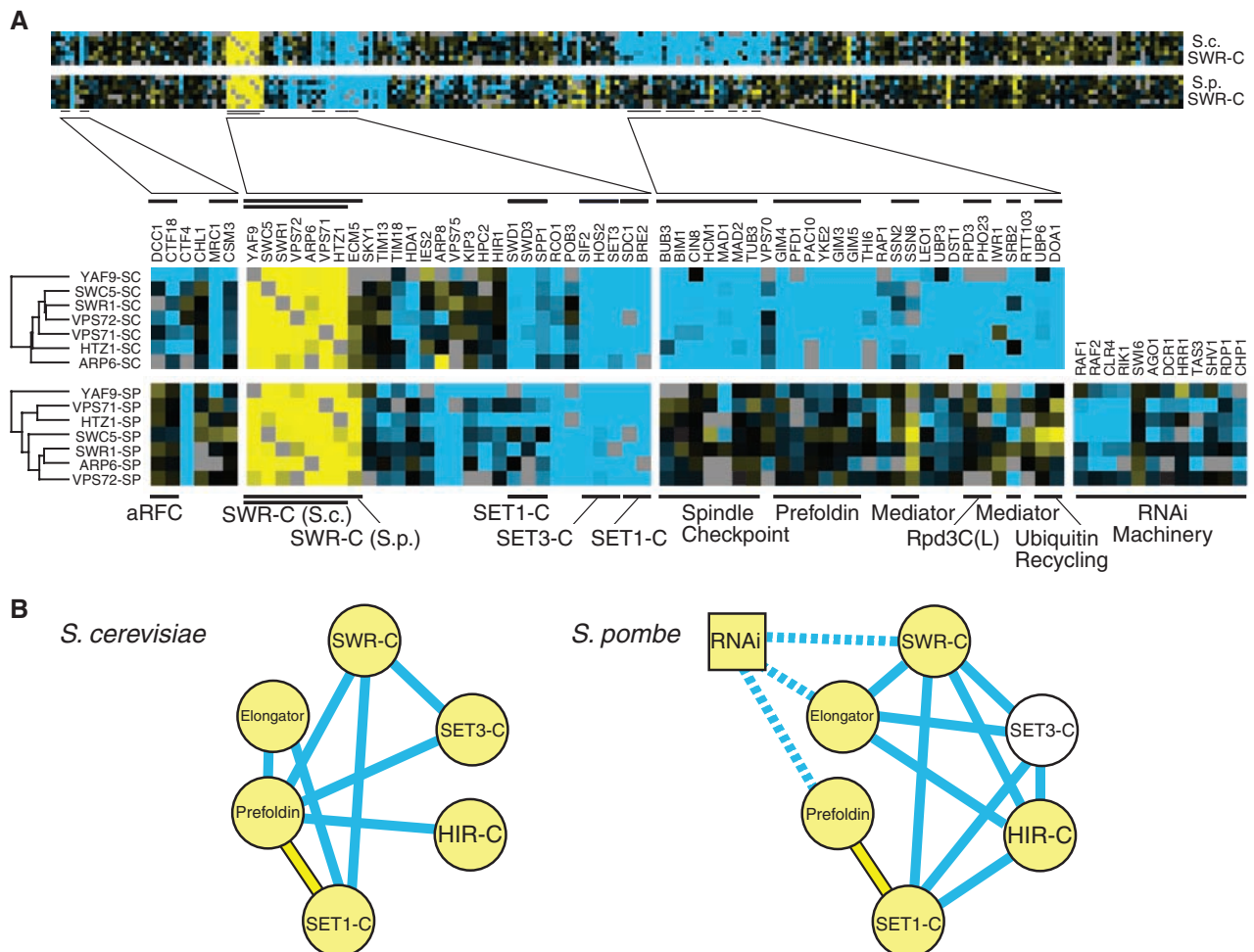


Fig. 5. Rewiring of the conserved functional modules. **(A)** Comparison of genetic interaction profiles of the SWR-C in *S. cerevisiae* and *S. pombe*. Analogous sets of genetic interactions from the two organisms are shown (database S2). **(B)** Genetic cross talk between functional modules. Modules are

represented as circles or boxes (in yellow if the interactions within the module are primarily positive). Negative and positive interactions between modules are represented as blue and yellow lines, respectively. The diagram was generated using the method described in (41).

interaction data from two evolutionarily distant species. Our data strongly support the idea that functional modules are highly conserved, but the wiring between them can differ substantially. Thus, the use of model systems to make inferences about biological network topology may be more successful for describing modules than for describing the cross talk between them.

References and Notes

1. M. Schuldiner *et al.*, *Cell* **123**, 507 (2005).
2. S. R. Collins *et al.*, *Nature* **446**, 806 (2007).
3. X. Pan *et al.*, *Methods* **41**, 206 (2007).
4. A. H. Y. Tong *et al.*, *Science* **303**, 808 (2004).
5. A. Roguev, M. Wires, J. S. Weissman, N. J. Krogan, *Nat. Methods* **4**, 861 (2007).
6. J. Tischler, B. Lehner, A. G. Fraser, *Nat. Genet.* **40**, 390 (2008).
7. Materials and methods are available as supporting material on Science Online.
8. S. R. Collins, M. Schuldiner, N. J. Krogan, J. S. Weissman, *Genome Biol.* **7**, R63 (2006).
9. C. Stark *et al.*, *Nucleic Acids Res.* **34**, D535 (2006).
10. R. Kaur, C. F. Kostrub, T. Enoch, *Mol. Biol. Cell* **12**, 3744 (2001).
11. J. Majka, P. M. Burgers, *Proc. Natl. Acad. Sci. U.S.A.* **100**, 2249 (2003).
12. A. Ghavidel *et al.*, *Cell* **131**, 915 (2007).
13. N. J. Krogan *et al.*, *Mol. Cell* **12**, 1565 (2003).
14. G. Mizuguchi *et al.*, *Science* **303**, 343 (2004), published 26 November 2003; 10.1126/science.1090701.
15. M. S. Kobor *et al.*, *PLoS Biol.* **2**, E131 (2004).
16. S. Ahmed, B. Dul, X. Qiu, N. C. Walworth, *Genetics* **177**, 1487 (2007).
17. A. Roguev *et al.*, *EMBO J.* **20**, 7137 (2001).
18. N. J. Krogan *et al.*, *J. Biol. Chem.* **277**, 10753 (2002).
19. A. Roguev *et al.*, *J. Biol. Chem.* **278**, 8487 (2003).
20. P. L. Nagy, J. Griesenbeck, R. D. Kornberg, M. L. Cleary, *Proc. Natl. Acad. Sci. U.S.A.* **99**, 90 (2002).
21. A. C. Gavin *et al.*, *Nature* **415**, 141 (2002).
22. A. Roguev *et al.*, *Mol. Cell. Proteomics* **3**, 125 (2004).
23. B. Dichtl *et al.*, *Mol. Cell* **10**, 1139 (2002).
24. S. I. Grewal, S. Jia, *Nat. Rev. Genet.* **8**, 35 (2007).
25. M. Zofall, S. I. Grewal, *Mol. Cell* **22**, 681 (2006).
26. T. Sugiyama *et al.*, *Cell* **128**, 491 (2007).
27. K. R. Hansen *et al.*, *Mol. Cell. Biol.* **25**, 590 (2005).
28. H. P. Cam, K. Noma, H. Ebina, H. L. Levin, S. I. Grewal, *Nature* **451**, 431 (2008).
29. N. J. Krogan *et al.*, *Nature* **440**, 637 (2006).
30. H. Spahr *et al.*, *J. Biol. Chem.* **275**, 1351 (2000).
31. H. Sakurai, M. Kimura, A. Ishihama, *Gene* **221**, 11 (1998).
32. D. N. Millband, K. G. Hardwick, *Mol. Cell. Biol.* **22**, 2728 (2002).
33. X. Liu, I. McLeod, S. Anderson, J. R. Yates III, X. He, *EMBO J.* **24**, 2919 (2005).
34. K. Asakawa *et al.*, *Mol. Biol. Cell* **17**, 1421 (2006).
35. I. M. Hall, K. Noma, S. I. Grewal, *Proc. Natl. Acad. Sci. U.S.A.* **100**, 193 (2003).
36. G. Otero *et al.*, *Mol. Cell* **3**, 109 (1999).
37. J. Gardiner, D. Barton, J. Marc, R. Overall, *Traffic* **8**, 1145 (2007).
38. M. Sipiczki, *Genome Biol.* **1**, REVIEWS1011 (2000).
39. C. J. Penkett, J. A. Morris, V. Wood, J. Bahler, *Nucleic Acids Res.* **34**, W330 (2006).
40. B. E. Dul, N. C. Walworth, *J. Biol. Chem.* **282**, 18397 (2007).
41. S. Bandyopadhyay, R. Kelley, N. J. Krogan, T. Ideker, *PLoS Comput. Biol.* **4**, e1000065 (2008).
42. We thank P. Beltrao and G. Cagney for critical reading of the manuscript; M. Wires and S. Forsburg for discussion; P. Kemmerer for setting up the web database; S. Wang, C. Wen, and D. Avdic for technical help; and F. Stewart for sharing unpublished data. This work was supported by NIH [National Institute of General Medical Sciences grant GM084279 (T.I. and N. J.K.)], the Sandler Family Foundation (N.J.K.), the Howard Hughes Medical Institute (J.S.W.), National Cancer Institute (S.I.G.), Center for Cancer Research (S.I.G.), and the California Institute of Quantitative Biology (N.J.K.).

Supporting Online Material

www.sciencemag.org/cgi/content/full/1162609/DC1

Materials and Methods

SOM Text

Figs. S1 to S5

Tables S1 to S8

References

Databases S1 to S4

1 July 2008; accepted 12 September 2008

Published online 25 September 2008;

10.1126/science.1162609

Include this information when citing this paper.

REPORTS

Current-Induced Spin-Wave Doppler Shift

Vincent Vlaminck and Matthieu Bailleul

Spin transfer appears to be a promising tool for improving spintronics devices. Experiments that quantitatively access the magnitude of the spin transfer are required for a fundamental understanding of this phenomenon. By inductively measuring spin waves propagating along a permalloy strip subjected to a large electrical current, we observed a current-induced spin wave Doppler shift that we relate to the adiabatic spin transfer torque. Because spin waves provide a well-defined system for performing spin transfer, we anticipate that they could be used as an accurate probe of spin-polarized transport in various itinerant ferromagnets.

Spin transfer—the transfer of angular momentum produced by a flow of electrons through an inhomogeneous magnetization configuration (1, 2)—has many potential applications for data storage and microwave electronics. It has been demonstrated recently in nanostructured multilayers [current-induced magnetic switching (3, 4) and precession (5, 6)] and extended magnetic strips [current-induced domain-wall motion (7, 8)]. It is usually difficult to measure the magnitude of the spin transfer with such experiments because they involve a complex spatio-temporal evolution of the magnetization (4, 8). As recently suggested, spin transfer can also

occur when an electrical current flows through a spin wave (9, 10), which has the advantage of being a system that is stationary both in time and space: The low-amplitude magnetization perturbation is entirely determined by the wave vector \vec{k} and pulsation ω of the spin wave (Fig. 1A), and the standard adiabatic gradient expression of spin transfer torque (STT) for continuously variable magnetization (11–14) results in a simple shift of the frequency of the spin wave (10, 15)

$$\Delta\omega_{\text{STT}} = \frac{P\mu_{\text{B}}}{-|e|M_{\text{s}}} \cdot \vec{J} \cdot \vec{k} \quad (1)$$

where P is the degree of spin polarization of the electrical current, μ_{B} is the Bohr magneton, \vec{J} is the electrical current density, e is the electron charge, and M_{s} is the saturation magnetiza-

tion. Although this current-induced frequency shift should not be confused with a true Doppler shift (16) that occurs, for example, when a detector is moved along the ferromagnet in which the spin wave propagates (17), it can be identified formally as the Doppler shift that would occur if the full electron system were simply drifting with respect to the lab frame with a velocity of $P\mu_{\text{B}}\vec{J}/-|e|M_{\text{s}}$, as suggested 40 years ago by Lederer and Mills (18).

We used a micrometer-sized version of the propagating spin wave spectroscopy (PSWS) technique (19–21). The microfabricated sample (Fig. 1, B and C) consisted of a permalloy ($\text{Ni}_{80}\text{Fe}_{20}$) strip [width (w) = 2 μm , thickness (t) = 20 nm], at the extremities of which four metal pads served to inject the current I_{dc} and measure the resistance. An external field H_0 ($\mu_0 H_0 \sim 1$ T, where μ_0 is the permeability of the vacuum) magnetized the permalloy strip out of plane so that spin waves propagated in the so-called magnetostatic forward volume waves (MSFVW) geometry (19, 20). Spin waves were emitted and detected with a pair of spin wave antennae (center-to-center distance $D = 7.7$ μm) located above the central part of the strip and connected to a 20-GHz vector network analyzer via coplanar waveguides (CPW). Each antenna consists of a sub-micrometer-sized meander terminated with a short circuit. In the operating principle of PSWS (Fig. 1E), a microwave current $i(\omega)$ is injected into one antenna and generates a microwave magnetic field $h(\omega)$ that couples to the spin wave modes $m(\omega, k)$. These spin waves propa-

Institut de Physique et Chimie des Matériaux de Strasbourg, UMR 7504 CNRS–Université Louis Pasteur, 23 Rue du Loess, 67034 Strasbourg Cedex 2, France.